Poly(ethylene terephthalate)–Poly(caprolactone) Block Copolymer. I. Synthesis, Reactive Extrusion, and Fiber Morphology

WEIMING TANG, N. SANJEEVA MURTHY, FRANK MARES, MILTON E. MCDONNELL, SEAN A. CURRAN

Research and Technology, AlliedSignal Inc., P.O. Box 1021, Morristown, New Jersey 07962-1021

Received 6 January 1999; accepted 3 May 1999

ABSTRACT: A novel poly(ethylene terephthalate)–poly(caprolactone) block copolymer (PET–PCL) is synthesized in a reactive twin-screw extrusion process. In the presence of stannous octoate, ring-opening polymerization of ϵ-caprolactone is initiated by the hydroxyl end groups of molten PET to form polycaprolactone blocks. A block copolymer with minimal transesterification is obtained in a twin-screw extruder as a consequence of the fast distributive mixing of ϵ-caprolactone into high melt viscosity PET and the short reaction time. The PET–PCL structure is characterized by IV, GPC, ^{1}H-NMR, and DSC. Fully drawn and partially relaxed fibers spun from PET–PCL are characterized by WAXD and SAXS. A substantial decrease in the oriented amorphous fraction appears to be the major structural change in the relaxed fiber that provides the fiber with the desired stress–strain characteristics. © 1999 John Wiley & Sons, Inc. J Appl Polym Sci 74: 1858–1867, 1999

Key words: PET–PCL block copolymers; twin-screw extrusion; ring-opening polymerization; ϵ-caprolactone

INTRODUCTION

Vehicle safety seat belts are currently made from polyethylene terephthalate (PET) fibers that are fully drawn and then partially relaxed (2.7%). These fibers have the desired tensile properties: a tenacity of at least 7.5 g/denier and an elongation at break of 14%. However, such PET fibers do not show optimal deformation characteristics, i.e., the stress–strain response required to match the performance of the seat belt with that of "air bags" in an integrated safety restraint system. Crash studies indicate that, after initial vehicle impact, the occupant will move forward from the seated position until the belt engages to build restraining forces. For a 35 mile/h crash, as indicated in Figure 1, the current relatively unyielding belt of PET fibers exerts a force of at least 2000 pounds (ca. 9000 Newtons) at 80 milliseconds against the occupant at the seat belt torso position with a potential for chest, rib cage, head, and neck injuries. An improved life-saving seat belt would substantially minimize occupant injuries.

Various technologies to improve occupant safety have been described in several U.S. patents.[1–13] These technologies include installation of mechanical or plastic energy-absorbing devices in the seat belt assembly, incorporation of elastic fibers as a secondary component in the seat belt, and changes in the weaving pattern of the fibers in the seat belt. A recent U.S. patent describes a new type of seat belt fiber spun from a poly(ethylene terephthalate)–poly(caprolactone) block copolymer, $[C(O)C_6H_4C(O)—OCH_2CH_2O]_m—[C(O)—(CH_2)_5—O]_n$, prepared in a reactive twin-screw extrusion process.[14] The safety seat belt made

Correspondence to: W. Tang.

Journal of Applied Polymer Science, Vol. 74, 1858–1867 (1999)
© 1999 John Wiley & Sons, Inc. CCC 0021-8995/99/071858-10

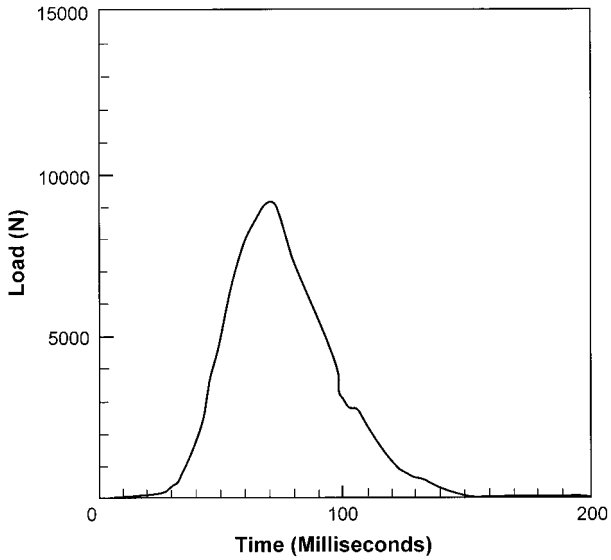

Figure 1 The performance of a seat belt made from PET fibers in a car-crash test. The ordinate axis refers to the load (N) against occupant, and the abscissa axis refers to the time (milliseconds) from the point of crash.

from this type of fiber provides the desired load-limiting performance. For a 35 mile/h crash, as indicated in Figure 2, the force against the occupant is reduced to less than 1400 pounds (ca. 6300 Newton) at 95 milliseconds. This type of energy-absorbing seat belt (Securus™, Allied Signal Inc.) reduces occupant injury and improves transportation safety.

The preparation of the poly(ethylene terephthalate)–poly(caprolactone) block copolymer (PET–PCL) and the process of fiber spinning were described in subsequent patent applications.[15–19] In this article, we detail polymer synthesis, reactive twin-screw extrusion, fiber morphology, and the block copolymer structure–property-processing relationships.

EXPERIMENTAL

Materials

Poly(ethylene terephthalate) (IV = 0.9 dL/g) was produced by AlliedSignal Polymers. Before use, the PET pellets were dried at 140°C *in vacuo* for at least 20 h. The moisture content, measured by the Karl-Fischer method, was less than 15 μg/g of PET. The effects of moisture on the polymerization are neglected in this article to simplify the discussion. High-grade ϵ-caprolactone (ECEQ) was purchased from Union Carbide Corporation. Stannous octoate was purchased from Elf Atochem North America Inc.

Characterization Techniques

Intrinsic Viscosity (IV)

The polymer solution viscosity was measured in a mixed solvent of 60 parts of phenol and 40 parts of tetrachloroethane at 25°C with a Ubbelohde glass viscometer. The polymer IV was determined by plotting the reduced specific viscosity of polymer solution vs. solution concentration. The intercept gave the polymer IV.

Gel Permeation Chromatography (GPC)

The apparent molecular weight and molecular weight distribution of PET–PCL were determined by GPC. The separation was performed at 35°C in a Waters Alliance 2690 system with two linear narrow bore Phenogel columns. The samples were eluted in a solvent mixture of chloroform/hexafluoro-2-propanol (98:2 volume) at a flow rate of 0.5 mL/min. A 10-μL aliquot of 0.05% polymer concentration was injected. The eluant was monitored at 254 nm and analyzed with Waters Millennium GPC software. The columns were calibrated with linear polystyrene. PET–PCL data

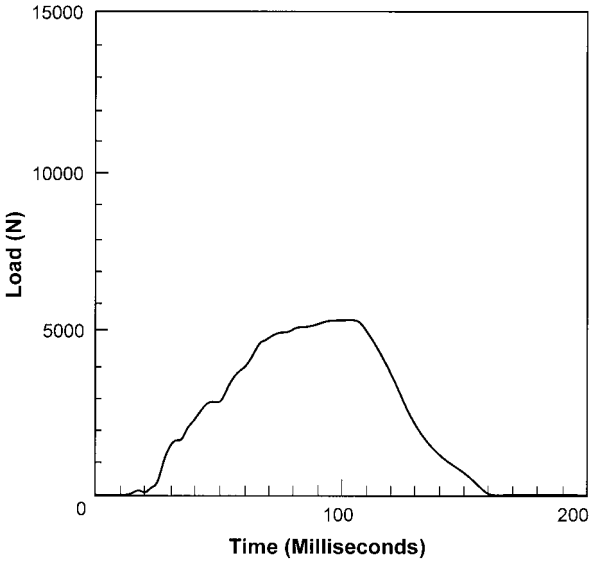

Figure 2 The performance of a seat belt made from PET–PCL fibers in a car-crash test. The ordinate axis refers to the load (N) against occupant, and the abscissa axis refers to the time (milliseconds) from the point of crash.

were analyzed by using the Mark Houwink coefficients to give the correct molecular weight.

Proton Nuclear Magnetic Resonance (^{1}H-NMR)

A single pellet (~5 mg) of PET–PCL was dissolved in 50/50 by weight deuterated chloroform and deuterated pentafluorophenol in a 5-mm NMR tube. ^{1}H-NMR spectra were run at 25°C on a Varian Unity Inova (Varian Instruments, Palo Alto, CA) NMR spectrometer with a ^{1}H operating frequency of 400 MHz. Sixteen scans were acquired with a recycle time of 10 s to achieve quantitative results.

Differential Scanning Calorimetry (DSC)

Thermal properties were measured under nitrogen in a Perkin-Elmer DSC-7 on a polymer chip of about 5 mg. The measurement sequence included heating the sample to 285°C at a rate of 10 K/min, holding the sample at 285°C for 2 min, and cooling the sample to 0°C at a rate of 10 K/min.

Wide-Angle X-ray Diffraction (WAXD)

WAXD data were collected on a Philips diffractometer with Cu Kα radiation and a graphite monochromator in the diffracted beam. The fibers were wound on a rectangular frame and covered an opening of 1 cm in diameter. The data were obtained by using two kinds of geometry. The data obtained in parafocus geometry, in which the instrumental broadening was small (0.09°), were used to calculate the crystallite sizes of the *hko* reflections. The data obtained in the transmission geometry with the sample spun in the plane of the fiber at a faster speed than the scanning speed (fast-rotational scan) were used to calculate the crystallinity. These data (2θ between 10 and 35°) were analyzed by resolving the scan into several crystalline peaks and two amorphous halos at 2θ ~20° and ~25°[20]

Crystalline orientations of the fibers were determined from the azimuthal widths of the 010, 100, and $\bar{1}05$ reflections in the two-dimensional data obtained by using an area detector (Bruker Analytical X-ray Systems, Inc.) and a small bundle of 50 filaments (filament dia. 20 μm) held tightly between v-grooves in a stiff frame. The degree of orientation f was calculated from the azimuthal angular width ($\Delta\phi$) of the peak in the azimuthal scan of the reflection.

Amorphous orientation of the fibers was determined from a sequence of 36 radial scans from ϕ = 0° (equator, +x) to ϕ = 180° (−x) on a curved positive sensitive detector (Inel Inc.) with θ set at 10° (half the 2θ value of the approximate position of the amorphous halo). Such an arrangement approximates the symmetrical transmission geometry ($\theta/2\theta$) at least for the amorphous halo. These radial scans were profile fitted to various crystalline peaks and two amorphous halos at 2θ ≈20° and 25°;[21] although three amorphous halos were required to completely describe the amorphous intensity distribution,[22] two were found to be adequate. The integrated intensity of the amorphous halo at 25° was plotted as a function of the azimuthal angle, and this curve was fitted to a baseline and a Gaussian peak.[23] A similar analysis of the 20° peak was difficult, and gave unreliable results, possibly because a mesophase also has a peak in this angular range.[24] The normalized area of the Gaussian peak represented the fraction of the oriented amorphous component, and the full-width at half maximum (fwhm) of the Gaussian peak was a measure of the degree of orientation of the oriented amorphous component.

Small-Angle X-ray Scattering (SAXS)

SAXS data were obtained at the National Synchrotron Light Source, Brookhaven National Laboratory (beam-line 27C, wavelength of 1.307 Å, a sample to detector distance of 168 cm). The lamellar spacing L was calculated from the Bragg spacing of the lamellar reflections. The tilt angle was calculated from the azimuthal angle between the lamellar reflections on either side of the fiber axis.

Tensile Properties

Stress–strain curves were measured on an Instron machine equipped with pneumatic cord and yarn grips that held the yarns at the gauge length of 10 inches. The yarn was then pulled at a strain rate of 10 inch/min under standard conditions (23 ± 2°C, 50 ± 5% relative humidity), and the data were recorded by a load cell. Tenacity was calculated as the breaking strength (in grams) divided by the yarn's denier (weight in gram of 9000 meters of yarn—a measure of fiber initial cross-section). Elongation at break was calculated as the ratio of the displacement at break to the initial gage length.

Reactive Twin-Screw Extrusion

The PET pellets were fed into a counterrotating twin-screw extruder (American Leistritz Com-

pany, diameter = 27 mm, screw rpm = 150, L/D = 48, Scheme 1) at a rate of 5.8 kg/h by a Ktron loss in weight feeder. The pellets were then heated to melt in the first two barrel sections (set temperature = 290°C). The melt was forwarded to an injection position where premixed ϵ-caprolactone and stannous octoate at the weight ratio of 1000:3.25 were injected by a piston pump at a rate of 1.0 kg/h. The PET melt and ϵ-caprolactone mixture formed a uniform mixture within 40 s, which was forwarded into a reaction zone where the set temperature was 260°C. Copolymerization was completed with a mean residence time of 4 min. Residual unreacted ϵ-caprolactone (~1 mol % of injected comonomer) was removed by vacuum at the devolatilization section, and condensed into a cold trap.

Fiber Spinning

The copolymer melt prepared in the twin-screw extruder was metered through a Zenith gear pump and directly fed into a spin pot that contained a filteration screen and a 50 round-hole spinnerette. After passing through a heated sleeve at 275°C, the extruded filaments were quenched with room-temperature air. A spin finish was applied and the fibers were taken up by a godet at a speed of 280 m/min. Then, the as-spun fibers were drawn with a draw ratio of 6.6:1 and annealed at 175°C to obtain fibers with high tenacity (PET–PCL Fiber, sample 1, 11.0 denier/filament). In the final stage, the fully drawn fiber was relaxed between the draw rolls and a last roll with 11% set speed difference to yield fibers (PET-PCL Fiber, sample 2, 12.4 denier/filament) with the desired stress–strain characteristics (Scheme 2).

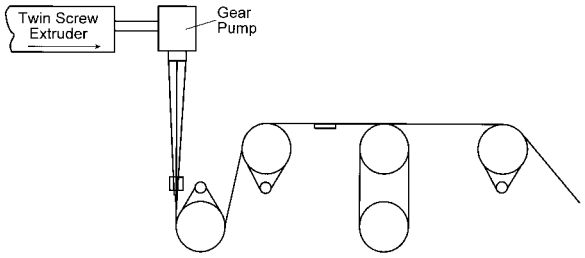

Scheme 2 The fiber spinning process for the production of PET–PCL fibers.

RESULTS AND DISCUSSIONS

Design of the Polymer

Design of novel PET–PCL block copolymer structure and optimization of fiber processing conditions allow us to prepare a fiber with the desired stress–strain characteristics. The interaction between PET and PCL chains in the amorphous region may result in a miscible phase with a single glass transition temperature between those of PET and PCL.[25,26] PET–PCL transesterification should be minimized to sustain the high molecular weight PET blocks required for high PET crystallinity and axial crystallite orientation in the new seat belt fiber.

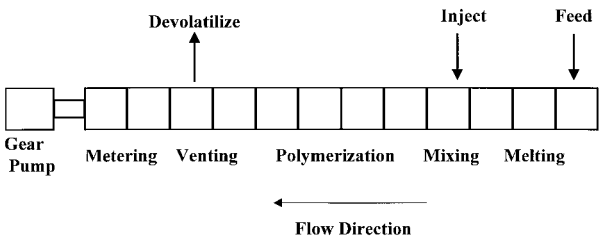

Scheme 1 The reactive twin screw extrusion process for the production of the PET–PCL block copolymer.

Polymer Synthesis

The PET end groups (IV = 0.9) were analyzed by ^{1}H-NMR spectroscopy and titration.[27,28] In ^{1}H-NMR spectra, the chemical shift at 4.10 ppm is assigned to the methylene protons next to the hydroxyl end group (—$CH_2C\underline{H}_2OH$). Titration of the PET carboxyl end groups gives an acid number of 24 mmol/kg. The acid number and the number-average molecular weight of PET (IV = 0.9, M_n = 31,200) allow us to estimate the hydroxyl end group concentration of 38 mmol/kg (Scheme 3).

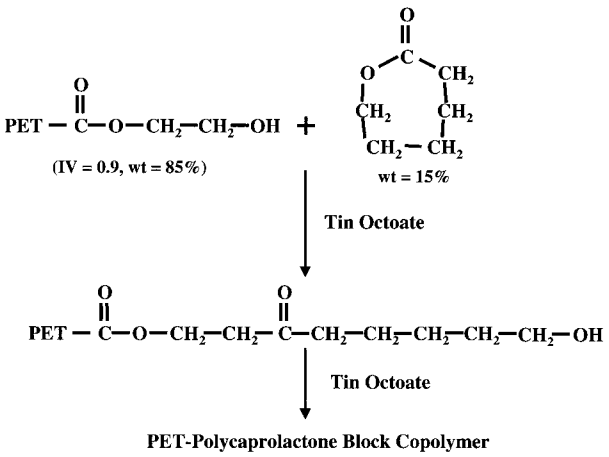

Scheme 3 The synthesis of the PET–PCL block copolymer.

The mechanism of ring-opening polymerization of ϵ-caprolactone has been proposed in the literature.[29] Stannous octoate is assumed to complex with ϵ-caprolactone and activate the comonomer toward the nucleophilic attack by the hydroxyl end groups of PET to generate an ω-hydroxy ester. The reaction propagates by continuous attack of the hydroxyl end groups of the polymer on ϵ-caprolactone to form polycaprolactone blocks. If 15 wt % of ϵ-caprolactone is reacted with 85 wt % of PET (IV = 0.9), one may estimate theoretically the number-average molecular weight of the polycaprolactone block to be ca. 4600 from

$$M_{n\,\text{theoretical}} = DP * M_w = \text{Mol}_{\text{CL}} * M_w/\text{Mol}_{\text{PET —OH end group}} \quad (1)$$

Here, DP is the degree of polymerization and is equal to monomer/initiator molar ratio. M_w is the molecular weight of ϵ-caprolactone. The IV of the resulting PET–PCL block copolymer is 1.0 dL/g.

Ring-opening polymerization in the presence of stannous octoate usually allows a controlled synthesis leading to polymers with a narrow molecular weight distribution (MWD).[30,31] If lactone backbiting transesterification occurred in the process, it formed cyclic lactone oligomers and a broadened MWD. GPC studies show the same breadth of MWD in PET–PCL as that of the original PET. Furthermore, soxhlet extractions by cyclohexane and 2-methoxyethyl ether yield 0.3 wt % and 5.7 wt % extractables from original PET–PCL, respectively. The ^{1}H-NMR and liquid chromatography studies of the extractable materials show no evidence of any cyclic lactone oligomers. Thus, the ϵ-caprolactone–PET copolymerization in the current process seems to occur without lactone backbiting transesterification.

Transesterification between PET and PCL modifies the block copolymer structure sequence by incorporating some lactone units into PET blocks and PET repeating units into PCL blocks.[32] The chemical shifts are solvent dependent, so all samples were run in the 50/50 $CDCl_3$/PFP mixed solvent. Based on the ^{1}H-NMR studies of homopolymers and model compounds, one can make some assignments for the ^{1}H-NMR spectrum in Figure 3 and Table I.[33,34] For example, in a homopolymer PET, the methylene protons adjacent to ether and ester in diethylene glycol terephthalate resonate at 4.15 and 4.53 ppm, respectively, while those in the ethylene glycol terephthalate resonate at 4.78 ppm.

The peak integration indicates that 27 mol % of the injected ϵ-caprolactone is scrambled into the PET blocks. In addition, 1 mol % of the injected ϵ-caprolactone is not reacted with the PET and is removed by the vacuum at the end of reactive extrusion process. Thus, PET–PCL transesterification reduces the number-average molecular weight of PCL to ca. 3300.

Thermal Analysis

The glass transition temperatures of PET and PCL homopolymers are ca. 80°C and ca. −60°C, respectively.[35] The DSC thermogram of PET–PCL (Fig. 4) shows that the glass transition temperature of the copolymer is ca 45°C. The single glass transition temperature in the copolymer and its shift indicate that PET and PCL are miscible in the amorphous phase. The melting temperature of PET–PCL is 230°C compared to 250°C in PET. The depression of melting temperature could be attributed to the transesterified caprolactone units which restrict PET crystallization, reduce PET crystallite size, subsequently increase surface free energy of crystallite and shorten thickness of lamellae. It may also be caused by the broadening of the interfacial region from the introduction of the PCL block.[36]

Reactive Twin-Screw Extrusion

The advantages of reactive twin-screw extrusion as a continuous PET–PCL production process are: (1) excellent dispersive and distributive mixing, (2) precise reaction temperature control, (3) short reaction time, and (4) efficient removal of unreacted monomer and volatile reaction byproducts.[37–39]

Since the viscosity ratio of ϵ-caprolactone and PET melt is 1 : 10^8, gear mixers[40,41] were chosen and assembled beneath the injection position to achieve distributive mixing. As a result, the melt flow is frequently split and reoriented under shear strain and elongational strain to achieve homogeneity within a short mixing time (e.g., 40 s). In the reaction zone, the exothermic polymerization of ϵ-caprolactone releases about 190 J/g heat of polymerization, which increases melt temperature by about 6°C. Because the screw elements in the reaction zone provide the desired extrusion free volume, and are completely filled with material, the reaction time is controlled by adjusting the throughput rate of the extruder.

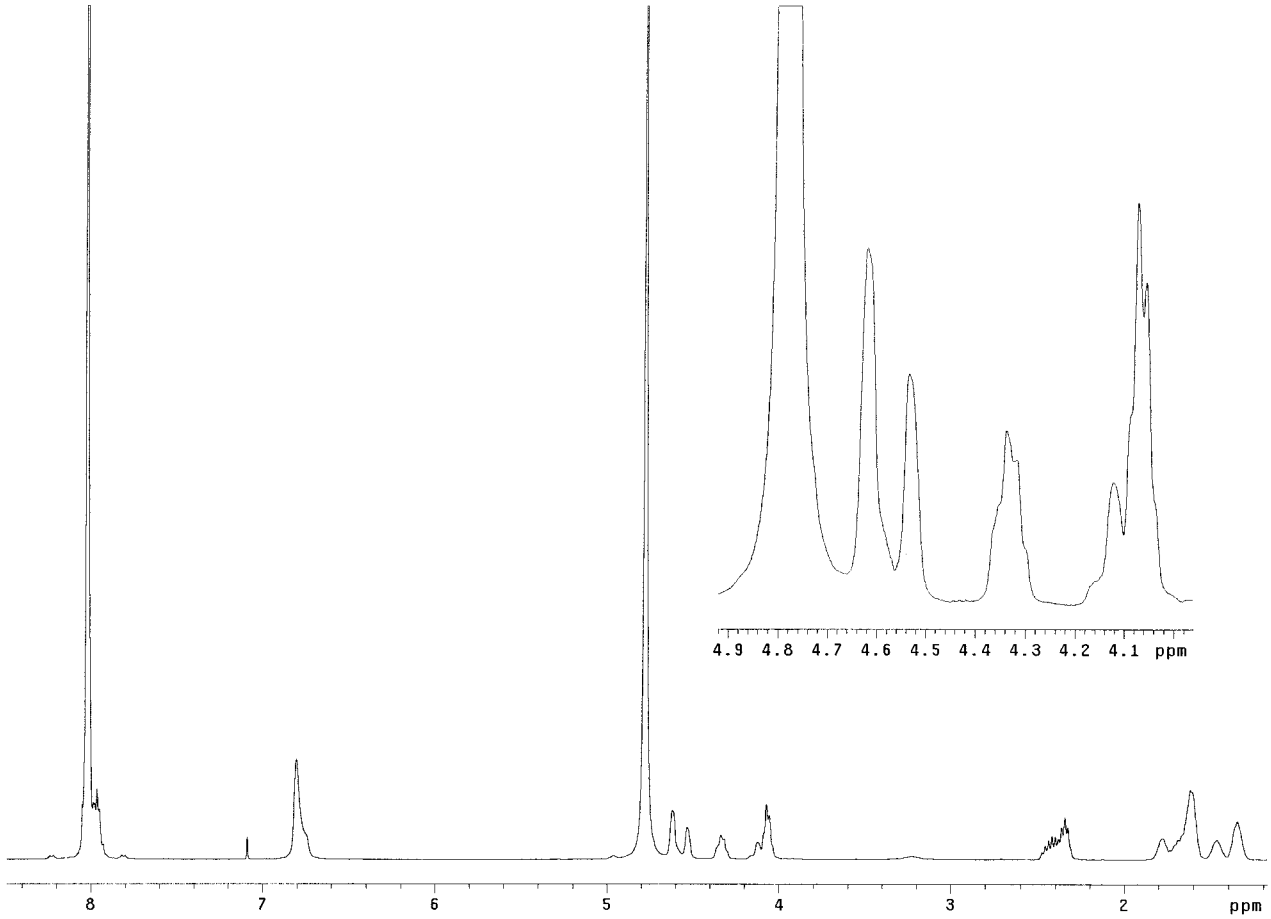

Figure 3 The ^{1}H-NMR spectrum of the PET–PCL block copolymer.

Crystalline Regions in PET–PCL Fibers

Examples of the WAXD data used in the characterization of the crystalline regions in PET–PCL fiber samples are shown in Figure 5. The crystallite sizes are calculated from equatorial (parafocus) and meridional scans [Fig. 5(a) and (b)]. Crystallinities are calculated from a fast rotational scan so as to eliminate the effect of orientation [Fig. 5(c)]. The results of the calculations are listed in Table II. The crystalline peaks are broader in the copolymer fiber than in the PET fiber. This means that the crystallites in the copolymer fiber are smaller than those in the PET fiber. The crystallinity and crystallite size of fully drawn and relaxed fibers (samples 1 and 2) are essentially the same. Therefore, the last relax-

Table I Resonances in the Range from 4.00 to 5.00 ppm in ^{1}H-NMR Spectrum of the PET–PCL Block Copolymer

Chemical Shift, ppm	Assignment
4.07	(—OC(O)C$\underline{H}_2$CH$_2$CH$_2$CH$_2$CH$_2$—)$_n$ in the PCL block
4.15	(OCH$_2$C$\underline{H}_2$OC$\underline{H}_2$CH$_2$O) in the PET block
4.34	(—OC(O)C$\underline{H}_2$CH$_2$CH$_2$CH$_2$CH$_2$—) in the caprolactone repeating unit scrambled into the PET block
4.53	(OC$\underline{H}_2$CH$_2$OCH$_2$C$\underline{H}_2$O) in the PET block
4.62	(OC$\underline{H}_2$C$\underline{H}_2$O) in ethylene glycol scrambled into the PCL block
4.78	(—C(O)C$_6$H$_4$C(O)OC$\underline{H}_2$C$\underline{H}_2$O—)$_n$ in the PET block

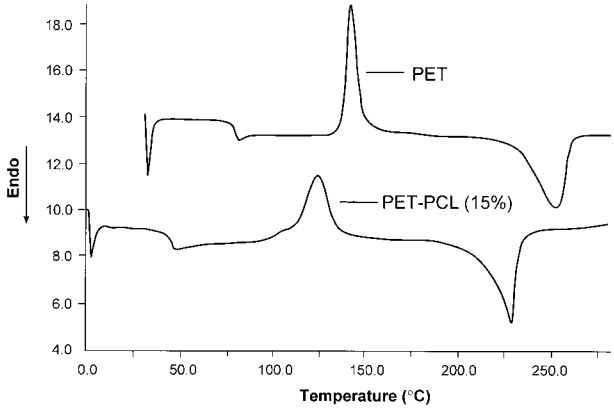

Figure 4 The DSC thermograms of the PET–PCL block copolymer and PET homopolymer.

ation step, which shrinks the fully drawn fibers, does not affect the characteristics of the crystalline domains.

The average value of crystalline orientation in the fully drawn sample reaches 0.987. The crystalline orientation of the relaxed fiber decreases to 0.976.

Amorphous Regions in PET–PCL Fibers

The amorphous phase in fibers can be described as comprised of oriented and unoriented components.[23,42,43] The integrated intensity of the amorphous halo at 25° is plotted as a function of the azimuthal angle, as shown in Figure 6. The area above the baseline is attributed to the oriented amorphous component, and the area below the baseline to the unoriented component. This kind of separation does not necessarily imply that there are two distinct domains of amorphous

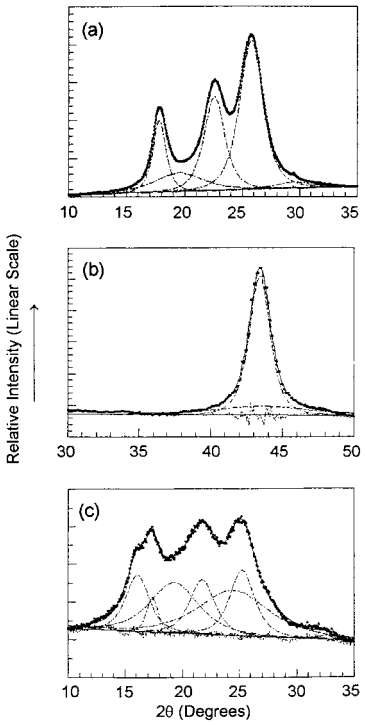

Figure 5 The profile analysis of the WAXD scans: (a) equatorial (parafocus) scans, (b) meridional (transmission) scans, and (c) fast-rotational (transmission) scans.

chains. It could be that there are small aggregates of oriented amorphous chains in a matrix of unoriented amorphous chains, or adjacent to the growth faces of axially oriented crystallites. It is quite possible that these aggregates are more prevalent in the interfibrillar regions than in the interlamellar regions. The data in Figure 6 are fitted to a baseline and a Gaussian peak. The area

Table II Summary of the WAXD and SASX Data

Sample	CI[a] %	CSP (Å)[b] 010	$\bar{1}10$	100	$\bar{1}05$	Cryst. Orientation[c] 010	100	$\bar{1}05$	Am. Orientation.[d] F	f	L Å	2ϕ[e] Degrees
Sample 1 (fully drawn)	45	59	37	34	51	0.987	0.986	0.989	0.553	0.867	144	119.6
Sample 2 (11% relaxed)	46	63	40	35	50	0.978	0.973	0.978	0.406	0.860	128	126.2

[a] Average of 32 samples of the PET–PCL is 43 with 1 σ of 3%.
[b] This measures the broadening due to both size and lattice disorder/strain. The 1 σ in these values from more than 30 samples is 3 to 5 Å.
[c] The 1 σ in these values is 0.002 to 0.005.
[d] F is the fraction of the oriented amorphous component and f is the degree of orientation of the oriented amorphous component.
[e] This is twice the angle of tilt of the lamellar plane.

of the Gaussian peak above the baseline, normalized to the total area of the azimuthal scan, is the fraction of the oriented amorphous component. The fwhm of the Gaussian peak corresponds to the degree of orientation of the oriented amorphous component.

Figure 6 shows that the amorphous peak in the partially relaxed fiber is somewhat broader, but the baseline is significantly higher. The change in the height of the baseline indicates that the most marked change from fully drawn to relaxed fibers is a large decrease in the fraction of the oriented amorphous phase. The fraction of oriented amorphous phase is 0.553 in the fully drawn fiber (sample 1), and decreases to about 0.406 upon relaxing the drawn fiber between draw and quench rolls. However, the degree of orientation of the oriented amorphous component remains essentially the same (0.867) in both the fully drawn and relaxed fibers.

Lamellar Structure

Figure 7 shows the SAXS patterns of fully drawn and partially relaxed fibers. The lamellar spacing is 144 Å in the fully drawn fiber and decreases to 128 Å in the 11% relaxed fiber. This decrease in lamellar spacing is accompanied by an increase in the tilt angle of the lamellar plane from 120 to 126°.

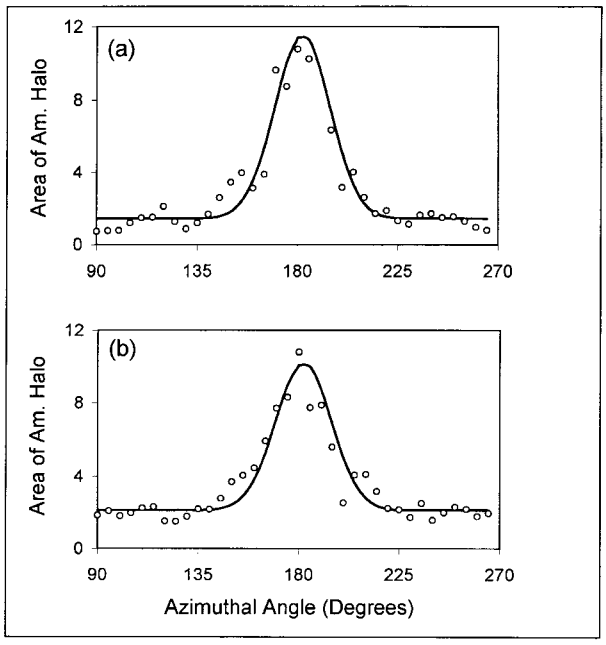

Figure 6 The azimuthal intensity distribution of the amorphous halo in (a) fully drawn fiber and (b) partially relaxed fiber.

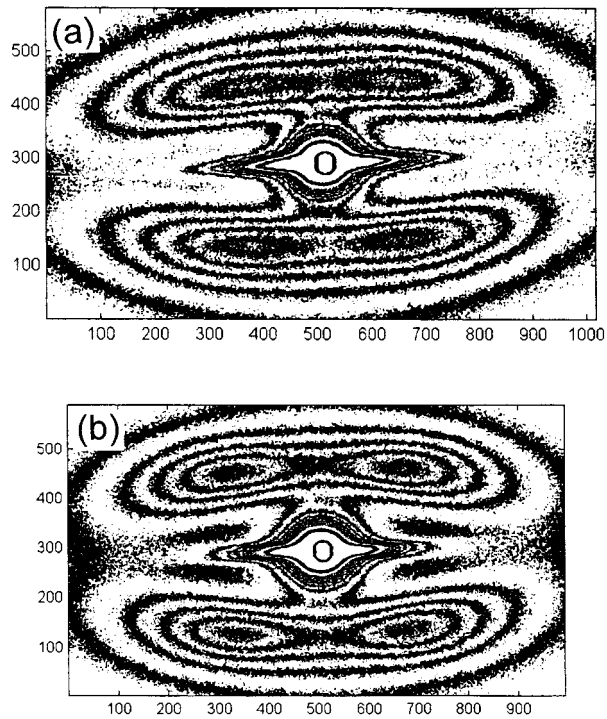

Figure 7 The SAXS data from (a) fully drawn fiber and (b) partially relaxed fiber.

Fiber Morphological Model

Based on the WAXD and SAXS studies, we propose the morphological model shown in Figure 8. The crystallinity value of 45% suggests that the fraction of the PET that crystallizes in PET–PCL fibers is the same as in PET fibers.

Fiber morphology undergoes dramatic changes during the drawing process. Under external stress, the amorphous polymer chains orient and crystallize in the draw direction. Subsequent relaxation of the fiber slightly decreases the crys-

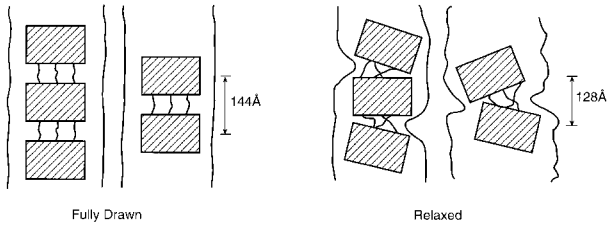

Figure 8 A proposed morphological model to illustrate the effect of fiber relaxation on the crystalline and amorphous orientation.

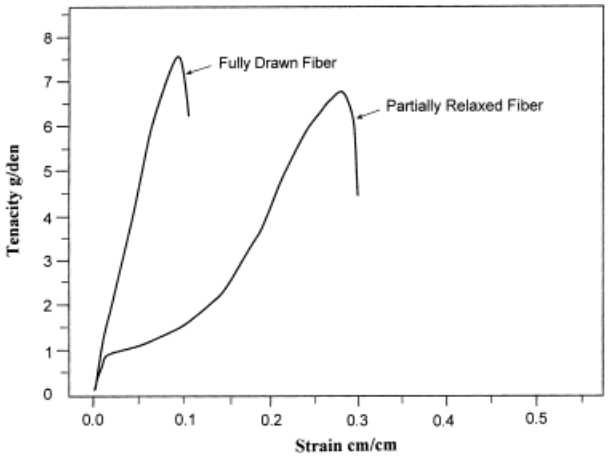

Figure 9 The stress–strain curves of PET–PCL fully drawn and partially relaxed fibers.

talline orientation, but brings about substantial changes in the amorphous regions. In our model, the high degree of amorphous orientation in the fully drawn fiber arises from the presence of elongated amorphous chain segments in the interfibrillar regions, and to a smaller extent between the lamellae within the fibrils. After the fibers are relaxed, some extended segments in the interfibrillar regions revert to the entropically favorable coiled state. The amorphous segments in the interlamellar regions are not as extended as those in the interfibrillar regions. Nevertheless, the conformation of the amorphous chains in the interlamellar regions becomes more coiled after the fiber relaxation. This is consistent with the decrease in the lamellar spacing and the increase in the tilt angle of the lamellar plane in our SAXS measurement. Thus, the increase in the fraction of the unoriented amorphous phase would modify the stress–strain curves of partially relaxed fiber from fully drawn fiber in Figure 9. In contrast to the fully drawn fiber, the deformation energy in the partially relaxed fiber is absorbed at a lower stress and a higher elongation. The fiber morphology and tensile properties determined by polymer structure and fiber processing conditions are critical factors to achieve the desired fiber for Securus™ (Allied Signal Inc.) load-limiting seat belt application.

CONCLUSIONS

The tensile characteristics of load limiting seat belt fibers were modulated by copolymerizing ϵ-caprolactone with PET to form the PET–PCL block copolymer, by processing the copolymer into fiber and tailoring morphology in the spin–draw–relax stages. This has resulted in a fiber with a high degree of crystalline orientation and a large fraction of the unoriented amorphous phase. These structural features provide a seat belt fiber that reduces occupant injury and improves transportation safety.

We thank our colleagues at AlliedSignal Polymer Technical Center (Petersburg, VA) and AlliedSignal Corporate Analytical Department (Morristown, NJ) for their support to this work. We are grateful to Dr. S. M. Aharoni for his comments on this article.

REFERENCES

1. Radke, D. G. U.S. Pat. 3,550,957.
2. Pickett, D. A.; Acs, S. N. U.S. Pat. 4,138,157.
3. Ballard, H. L. U.S. Pat. 3,530,904.
4. Truslow, N. U.S. Pat. 3,296,062.
5. Ballard, H. L. U.S. Pat. 3,464,459.
6. Seo, K; Hayashi, Y.; Hashino, T.; Masuda, F. U.S. Pat. 3,756,288.
7. Takada, T. U.S. Pat. 3,872,895.
8. Takada, T. U.S. Pat. 3,926,227.
9. Kikuchi, K. U.S. Pat. 4,228,829.
10. Koseki, T. U.S. Pat. 5,376,440.
11. Imamura, T. U.S. Pat. 4,710,423.
12. Stoffel, R. W.; Stevenson, W. U.S. Pat. 3,486,791.
13. Miller, H. J.; Dybro, N. U.S. Pat. 5,547,143.
14. Tang, W.; Mares, F.; Morgan, R. U.S. Pat. 5,830,811.
15. Tang, W.; Mares, F.; Morgan, R. U.S. Pat. 5,869,582.
16. Tang, W.; Mares, F.; Morgan, R. U.S. Pat. pending.
17. Tang, W.; Mares, F. U.S. Pat. pending.
18. Tang, W.; Mares, F.; Rahman, Z.; Nagy, M. U.S. Pat. pending.
19. Tang, W.; Mares, F. U.S. Pat., to be filed.
20. Murthy, N. S.; Minor, H. Polymer 1990, 31, 996.
21. Murthy, N. S.; Bednarczyk, C.; Rim, P. B.; Nelson, C. J. J Appl Polym Sci 1996, 64, 1363.
22. Murthy, N. S.; Zero, K.; Minor, H. Macromolecules 1994, 27, 1484.
23. Murthy, N. S.; Minor, H.; Bednarczyk, C.; Krimm, S. Macromolecules 1993, 26, 1712.
24. Auriemma, F.; Corradini, P.; De Rosa, C.; Guerra, G.; Petraccone, V.; Bianchi, R.; Di Dino, G. Macromolecules 1992, 25, 2490.
25. Ma, D.; Luo, X.; Zhang, R.; Nishi, T. Polymer 1996, 37, 1575.
26. Denchev, Z.; Bojkova, A.; DuChesne, A.; Stamm, M.; Fakirov, S.; Keul, H.; Höcker, H. Macromol Chem Phys 1998, 199, 2153.

27. Duda, A.; Florjanczyk, Z.; Hofman, A.; Slomkowski, S.; Penczek, S. Macromolecules 1990, 23, 1640.
28. Dubois, Ph.; Jacobs, C.; Jerome, R.; Teyssie, Ph. Macromolecules 1991, 24, 2266.
29. Kricheldorf, H. R.; Kreiser-Saunders, I.; Boettcher, C. Polymer 1995, 36, 1253.
30. Montaudo, G.; Montaudo, M. S.; Puglisi, C.; Samperi, F.; Spassky, N.; LeBorgne, A.; Wisniewski, M. Macromolecules 1996, 29, 6461.
31. Lofgren, A.; Albertsson, A. C.; Dubois, Ph.; Jerome, R. JMS Rev Macromol Chem Phys 1995, C35, 379.
32. Kricheldorf, H. R.; Berl, M.; Scharnagl, N. Macromolecules 1988, 21, 286.
33. Trollsås, M.; Atthoff, B.; Claesson, H.; Hedrick, J. L. Macromolecules 1998, 31, 3439.
34. Ma, D; Zhang, G.; Huang, Z.; Luo, X. J Polym Sci Part A Polym Chem 1998, 36, 2961.
35. Storey, R. F.; Herring, K. R.; Hoffman, D. C. J Polym Sci Part A Polym Chem 1991, 29, 1759.
36. Tang,W.; Farris, R. J.; MacKnight, W. J.; Eisenbach, C. D. Macromolecules 1994, 27, 2815.
37. Xanthos, M. Reactive Extrusion: Principles and Practice; Hanser Publishers: Munich, 1992.
38. Todd, D. B. Plastic Compounding; Hanser Publishers: Munich, 1998.
39. White, J. L. Twin Screw Extrusion; Hanser Publishers: Munich, 1990.
40. Manas-Zloczower, I.; Tadmor, Z. Mixing and Compounding of Polymers; Hanser Publishers: Munich, 1994.
41. Rauwendaal, C. Polymer Mixing; Hanser Publishers: Munich, 1998.
42. Wu, G.; Jiang, J.-D.; Tucker, P. A.; Cuculo, J. A. J Polym Sci Polym Phys 1996, 34, 2035.
43. Aharoni, S. M. Polym Adv Technol 1998, 9, 169.